Junctional actin assembly is mediated by Formin-like 2 downstream of Rac1

Katharina Grikscheit, Tanja Frank, Ying Wang, and Robert Grosse

Institute of Pharmacology, Biochemical-Pharmacological Center (BPC), University of Marburg, 35032 Marburg, Germany

Epithelial integrity is vitally important, and its deregulation causes early stage cancer. De novo formation of an adherens junction (AJ) between single epithelial cells requires coordinated, spatial actin dynamics, but the mechanisms steering nascent actin polymerization for cell–cell adhesion initiation are not well understood. Here we investigated real-time actin assembly during daughter cell–cell adhesion formation in human breast epithelial cells in 3D environments. We identify formin-like 2 (FMNL2) as being specifically required for actin assembly and turnover at newly formed cell–cell contacts as well as for human epithelial lumen formation. FMNL2 associates with components of the AJ complex involving Rac1 activity and the FMNL2 C terminus. Optogenetic control of Rac1 in living cells rapidly drove FMNL2 to epithelial cell–cell contact zones. Furthermore, Rac1-induced actin assembly and subsequent AJ formation critically depends on FMNL2. These data uncover FMNL2 as a driver for human epithelial AJ formation downstream of Rac1.

Introduction

Cell-to-cell adhesion is one of the hallmarks of the epithelium, which is found disrupted in many cancers during malignant transformation (Niessen et al., 2011). The connection between adherens junction (AJ) complexes and the actin cytoskeleton has long been appreciated, but how actin is assembled and regulated during de novo cell–cell contact formation under physiological conditions such as 3D environments is not well understood (Weis and Nelson, 2006; Ratheesh and Yap, 2012). Actin remodeling is essential not only for AJ formation and expansion, but also during junctional maintenance when actin turnover at cell–cell contacts reaches a steady state (Ivanov et al., 2005; Cavey and Lecuit, 2009). Thus, actin nucleation and polymerization appear highly specialized and dynamically regulated at the AJ. The Arp2/3 complex is involved in the regulation of junctional actin polymerization (Kovacs et al., 2011; Tang and Brieher, 2012); however, evidence for a role of formins, the largest group of actin nucleators, remains poorly understood (Michael and Yap, 2013).

Formins are multidomain proteins, controlled through intramolecular interaction of their C-terminal, Diaphanous autoregulatory domain (DAD) to the N terminus (NT). The current model of activation involves binding of active RhoGTPases to the RhoGTP binding domain (GBD), thereby releasing autoinhibition (Baarlink et al., 2010; Breitsprecher and Goode, 2013). Formin-1, which lacks an apparent GBD, was shown to modulate AJs in mouse keratinocytes (Kobielak et al., 2004; Campellone and Welch, 2010), whereas RhoA/Dia1/myosin II activity was proposed to strengthen AJs in a monolayer cell culture (Carramusa et al., 2007). However, a role for formins-mediated actin dynamics in the de novo formation of AJs in human epithelial cells in real time has not been addressed. Moreover, how experimental approaches to studying monolayer cells grown on rigid surfaces can be translated into more physiological 3D environments remains unclear (Baker and Chen, 2012; Kutys et al., 2013). A suitable model system is human MCF10A breast epithelial cells cultured in 3D Matrigel, which resembles components of a basement membrane (Debnath and Brugge, 2005).

Here we report that formin-like 2 (FMNL2) controls junctional actin assembly and turnover during initial AJ formation as well as epithelialization in 3D environments. FMNL2 associates with components of the AJ complex in a regulated fashion in which Rac1 promotes rapid and dynamic localization of FMNL2 and subsequent actin assembly at newly forming cell–cell contacts.

Correspondence to Robert Grosse: robert.grosse@staff.uni-marburg.de

Abbreviations used in this paper: AJ, adherens junction; CT, C terminus; DAD, Diaphanous autoregulatory domain; NT, N terminus.

The Rockefeller University Press $30.00
J. Cell Biol. Vol. 209 No. 3 367–376
www.jcb.org/cgi/doi/10.1083/jcb.201412015

Results and discussion

FMNL2 localizes to newly formed cell–cell contacts

MCF10A cells develop into a two-cell stage within the first 24 h when seeded into Matrigel. Within 2 wk they grow into larger spheroids, and lumen formation occurs via apoptosis of the inner cells (Debnath and Brugge, 2005; Fig. 1 A).

To analyze de novo junctional actin formation, we aimed at visualizing actin assembly during early stages of spheroid development in 3D, as represented by pairs of daughter cells (Fig. 1 A and Video 1). Live imaging of E-Cadherin–GFP and LifeAct-mCherry–expressing MCF10A cells allowed for visualization of actin dynamics and the formation of a native AJ immediately after cytokinesis (Fig. 1 B and Video 1). In mature cell pairs, phalloidin-based F-actin staining was uniformly distributed along the plasma membrane, including a circumferential actin ring characteristic of epithelial cells (Zhang et al., 2005), whereas E-Cadherin predominantly labeled the adhesion zone connecting two daughter cells (Fig. 1 C).

To identify formins involved in junctional actin regulation, we generated a formin mRNA expression profile, with Dia1 being the most abundant formin followed by FMNL2, whereas formin-1 and -2, FMNL3, or INF1 and -2 were low in MCF10A cells (Fig. 1 D). In our human 3D epithelial cell culture, endogenous Dia1 (also called mDia1 or DIAPH1) was absent from the AJ but displayed diffuse cytoplasmic localization (Fig. 1 E). In contrast, endogenous FMNL2 appeared to be enriched in the vicinity of cell–cell contacts (Fig. 1 E). Consistent with this, FMNL2-GFP localized to the AJ, colocalizing with E-Cadherin (Fig. 1 F). Interestingly, time-lapse analysis of FMNL2-GFP–expressing cells revealed that FMNL2 is recruited to early cell–cell contacts, accompanied by an increase in junctional F-actin as visualized by LifeAct (Fig. 1 G and Video 2).

We wanted to examine if FMNL2 is involved in actin assembly at cell–cell contacts. FMNL2 is autoinhibited, as mediated through the interaction of its DAD-containing C terminus (CT) and the NT. According to a previous report (Vaillant et al., 2008), we deleted the DAD region to generate an active FMNL2ΔDAD. Interestingly, FMNL2ΔDAD-GFP dominantly localized to cell–cell contacts, leading to increased F-actin when compared with GFP-expressing cells, indicating that junctional actin is assembled by FMNL2 activity (Fig. 1, H–J).

FMNL2 is required for de novo junctional actin formation

To investigate the role of FMNL2 in junctional actin, we made use of an inducible shRNA system (Meerbrey et al., 2011) to suppress FMNL2 (Fig. 2 A). Control shRNA-expressing cells co-transduced with LifeAct-GFP revealed stable junctional actin in live cell recordings (Fig. 2 B). Strikingly, in cells depleted of FMNL2, junctional F-actin appeared to be discontinuous and disrupted, supporting a role for FMNL2 in F-actin dynamics and integrity at AJs in 3D cell culture (Fig. 2, B and C; and Videos 3 and 4). To verify the specificity for FMNL2, we knocked down various formins expressed in MCF10A cells (Fig. S1 A) and tested their effect on Lifeact-GFP in living cells. No other tested formin exhibited disregulated junctional actin as well as reduced plasma membrane/cell contact F-actin ratios (Fig. 2 D and Fig. S1 B). Notably, in Lifeact-mCherry–expressing cells, depletion of FMNL2 and stable reexpression of active FMNL2ΔDAD rescued junctional F-actin formation (Fig. 2 E and Fig. S1 C), demonstrating a requirement for FMNL2 activity at cell–cell contacts.

To further address the role of FMNL2 in the dynamic regulation of junctional actin in living cells in Matrigel, we performed FRAP experiments (Fig. 2 F). The recovery curve of GFP-actin showed biphasic characteristics, as observed in other systems (Tardy et al., 1995; Fig. 2 G). The first phase ($t_{1/2}$_1) likely represents replenishment of free monomeric actin and initial nucleation/polymerization followed by a second, slower phase ($t_{1/2}$_2), which resembles actin monomer incorporation into the F-actin pool (Tardy et al., 1995). By applying the F-actin stabilizing drug Jasplakinolide, the G-actin pool appeared to be diminished, correlating with a reduced GFP-actin turnover. In contrast, sequestering of actin monomers using Latrunculin B accelerated initial GFP-actin recovery at the cell–cell contact (Fig. 2 G). Interestingly, in cells with reduced FMNL2 expression as well as inhibition of the Arp2/3 complex, we also observed an increase in initial fluorescence recovery of junctional actin (Fig. 2 H and Fig. S1, D–F). These data suggest that by decreasing actin polymerization, the G/F-actin equilibrium is shifted to an increase of monomeric G-actin. The impact of FMNL2 on junctional actin appeared to be specific, as cytoplasmic or plasma membrane GFP-actin pools were not affected (Fig. 2 I). siRNA-mediated silencing of Dia1 had no effect on junctional actin recovery as compared with FMNL2-depleted cells (Fig. S1 E). Together, these findings point toward a specific role for FMNL2 in regulating actin at the junctional membrane under 3D conditions.

Next, we examined the effects of long-term FMNL2 depletion on de novo epithelial lumen formation. To this end, inducible shFMNL2 cell lines were grown in a chemically inert 3D hydrogel. After 14 d, cells were stained for F-actin and the development of differentiated lumen was determined (Fig. 2 J). MCF10A as well as Caco2 cells transduced with shRNA against FMNL2 formed spheroids with a significantly higher incidence of impaired lumen formation compared with control cells (Fig. 2, J–M; and Fig. S1 I), demonstrating a requirement for FMNL2 in breast and colon epithelialization. Consistently, it was recently shown that FMNL2 is strongly detectable in human breast as well as colon epithelium (Gardberg et al., 2010). MCF10A cells expressing shRNA against FMNL2 showed no significant changes in proliferation (Fig. S1 H), which suggests that hyperproliferation or failure of apoptosis are not responsible for the observed phenotype. In addition, active FMNL2ΔDAD-GFP (Fig. 1 H) remained at AJs throughout lumen formation (Fig. S1 I), supporting a specific role for regulating actin assembly during epithelialization. However, FMNL2-depleted cells showed a reduced polarization toward the wound edge (Fig. S1 J), indicating that deregulation of polarity may contribute to the overall lumen phenotype.

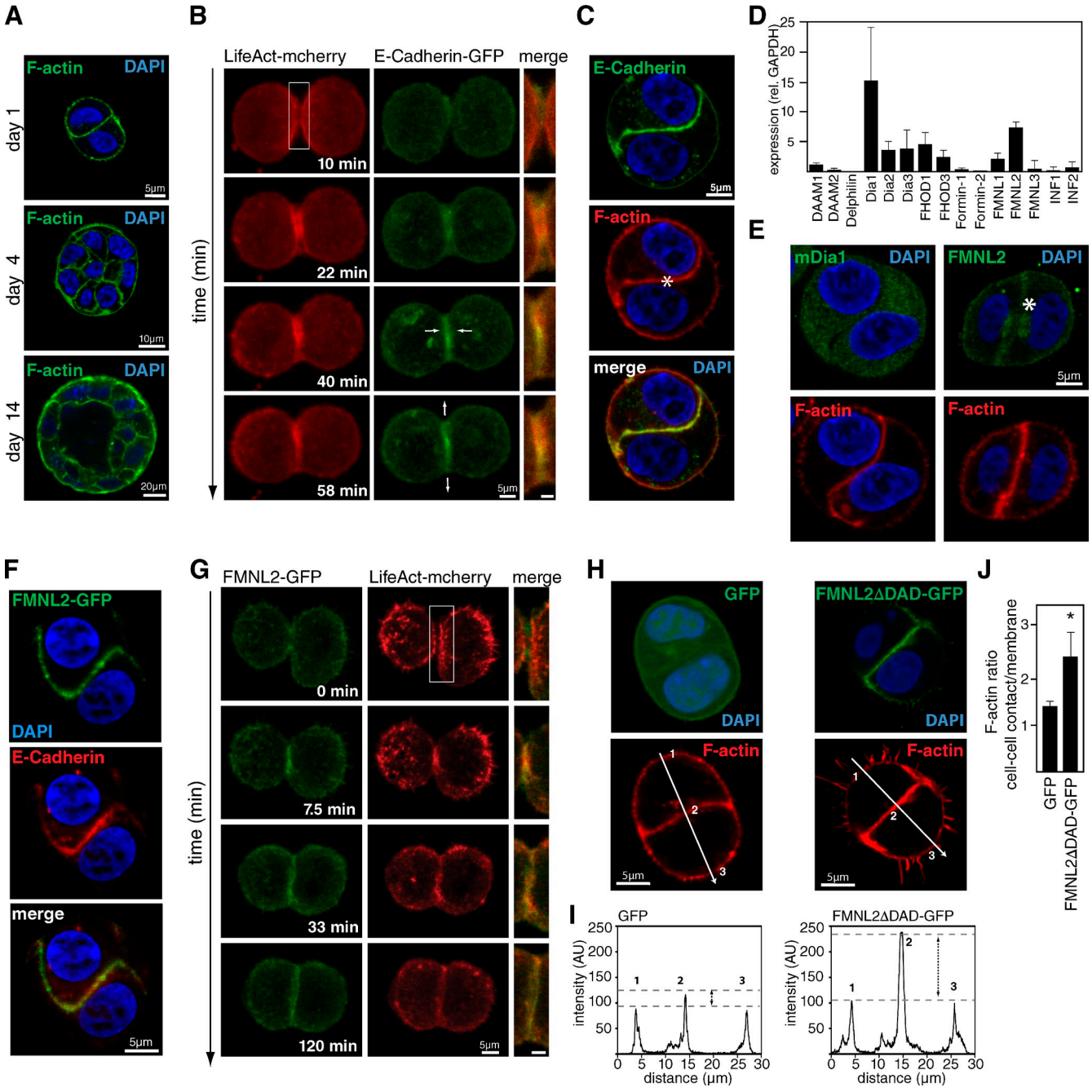

Figure 1. **FMNL2 localizes to AJs in a 3D model for nascent cell–cell adhesion formation.** (A) Confocal images of MCF10A cells in 3D stained for F-actin after 1, 4, or 14 d. (B) 3D reconstructions of MCF10A cells expressing LifeAct-mCherry and E-Cadherin–GFP during cell–cell contact formation. Merged images show magnification (bar, 2 µm). (C) MCF10A cells grown in Matrigel and labeled as indicated. The asterisk marks the junctional area. (D) Expression of formins in MCF10A cells assessed by qPCR. (E) MCF10A cells grown in Matrigel were labeled as indicated. FMNL2 localizes to the AJ (asterisk). (F) MCF10A cells expressing FMNL2-GFP were labeled for E-Cadherin. (G) 3D reconstructions of a time series of MCF10A cells expressing LifeAct-mCherry and FMNL2-GFP. Merged images magnify the AJ area (bar, 2 µm). (H) Representative images of MCF10A cells expressing GFP or FMNL2ΔDAD-GFP stained for F-actin. Arrows illustrate line scans used for quantifications. (I) Corresponding line scan profiles to H. (J) Quantification of F-actin line scan profiles (GFP, $n = 47$; FMNL2ΔDAD-GFP, $n = 66$). *, $P \leq 0.05$. Error bars indicate SEM.

FMNL2 associates with components of the AJ complex

The intracellular components of the AJ complex have been shown to actively shape the actin cytoskeleton by recruitment and activation of regulators such as Rac1, the Arp2/3 complex, or Tiam1 (Kraemer et al., 2007). Rac1 is well established to be localized to AJs in monolayer cell culture (Jou and Nelson, 1998; Nakagawa et al., 2001). As FMNL2 is localized to the area of native cell–cell contacts, we examined whether FMNL2 might be physically associated with the AJ complex and found that FMNL2 coimmunoprecipitated with endogenous E-cadherin, which was robustly increased when active Rac1 (RacL61) was

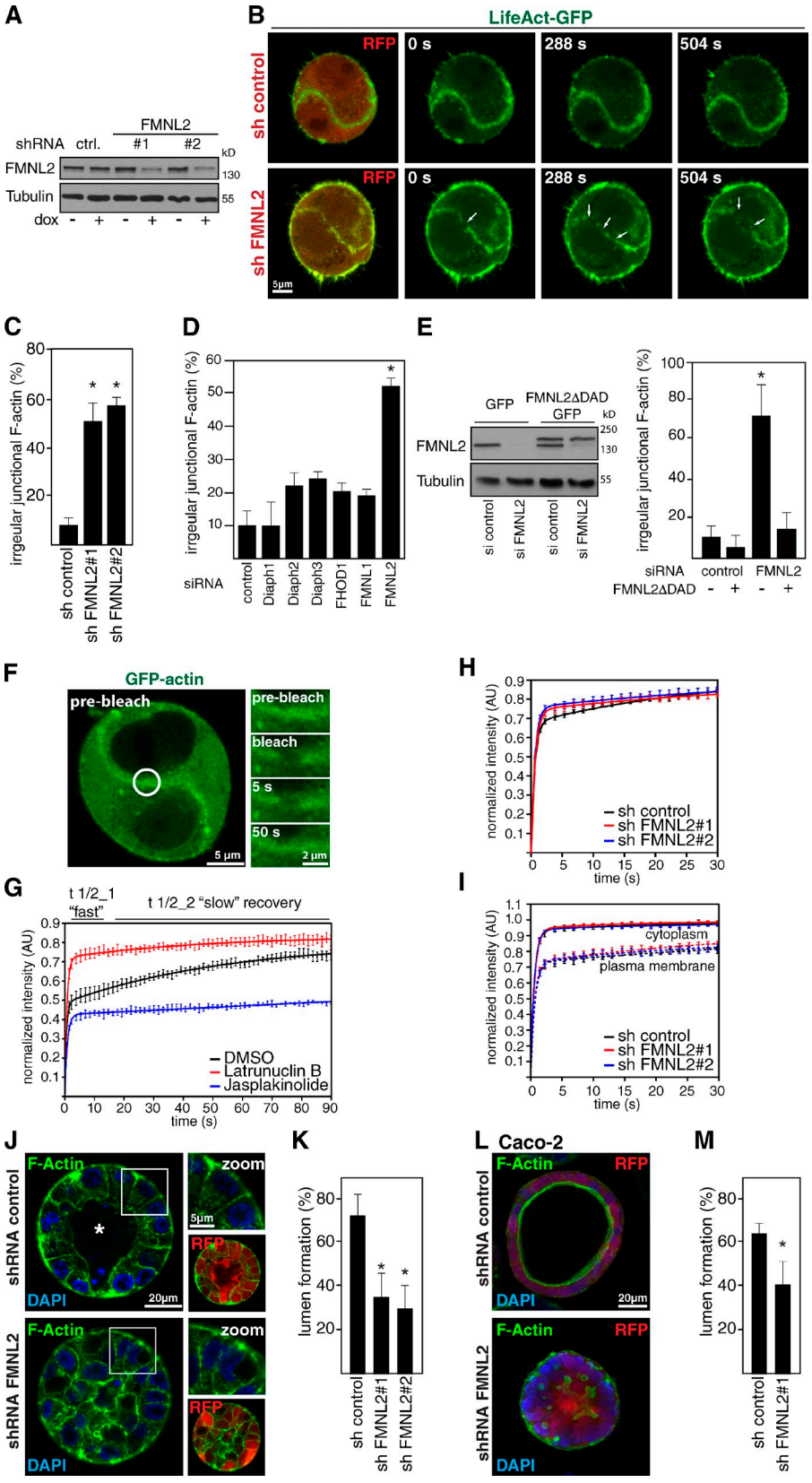

Figure 2. **FMNL2 is required for actin turnover at the cell–cell interface.** (A) Western blot analysis of MCF10A cells expressing dox-inducible control or FMNL2 shRNAs. (B) Live MCF10A cells expressing LifeAct-GFP with the indicated shRNAs (monitored through RFP) seeded in Matrigel. Arrows highlight the altered distribution of actin in FMNL2 shRNA cells. (C and D) Quantification of aberrant junctional actin as visualized by Lifeact-GFP in shRNA-expressing (C) or siRNA-treated (D) MCF10A cell pairs. (E) Western blot showing that FMNL2ΔDAD-GFP is resistant to siRNA against FMNL2 UTR. Active FMNL2 rescues junctional actin in FMNL2-depleted MCF10A cells in 3D. (F) MCF10A cell pair expressing GFP-actin. In 3D FRAP experiments, junctional GFP-actin was photobleached (white circle). Magnifications illustrate GFP-actin recovery. (G) FRAP curves comparing the effects of DMSO, Jasplakinolide, or Latrunculin B on junctional actin. (H) FRAP curves of GFP-actin MCF10A cells expressing indicated shRNAs. (I) Corresponding experiments to Fig. 2 F showing FMNL2-independent recovery of cytosolic and plasma membrane GFP-actin. (J) MCF10A cells expressing the indicated shRNAs grown for 14 d before staining for F-actin. The top right panels show an enlargement of individual cells. The bottom right panels show shRNAs as RFP. (K) Quantification of J. (L) Caco-2 cells expressing either control or FMNL2 shRNA grown in 3D for 7 d. After staining for F-actin, lumen formation was quantified (M). Error bars indicate SEM. *, $P \leq 0.05$.

expressed (Fig. 3 A), suggesting a regulated association of FMNL2 with the AJ. This association was confirmed by reciprocal coimmunoprecipitation of E-Cadherin with endogenous FMNL2 (Fig. 3 B).

Ectopically expressed FLAG-FMNL2 also associated with E-Cadherin–GFP mediated through its CT comprising the FH2 domain necessary for actin polymerization (Fig. 3 C). Given the Rac-mediated nature of this association (Fig. 3 A), we

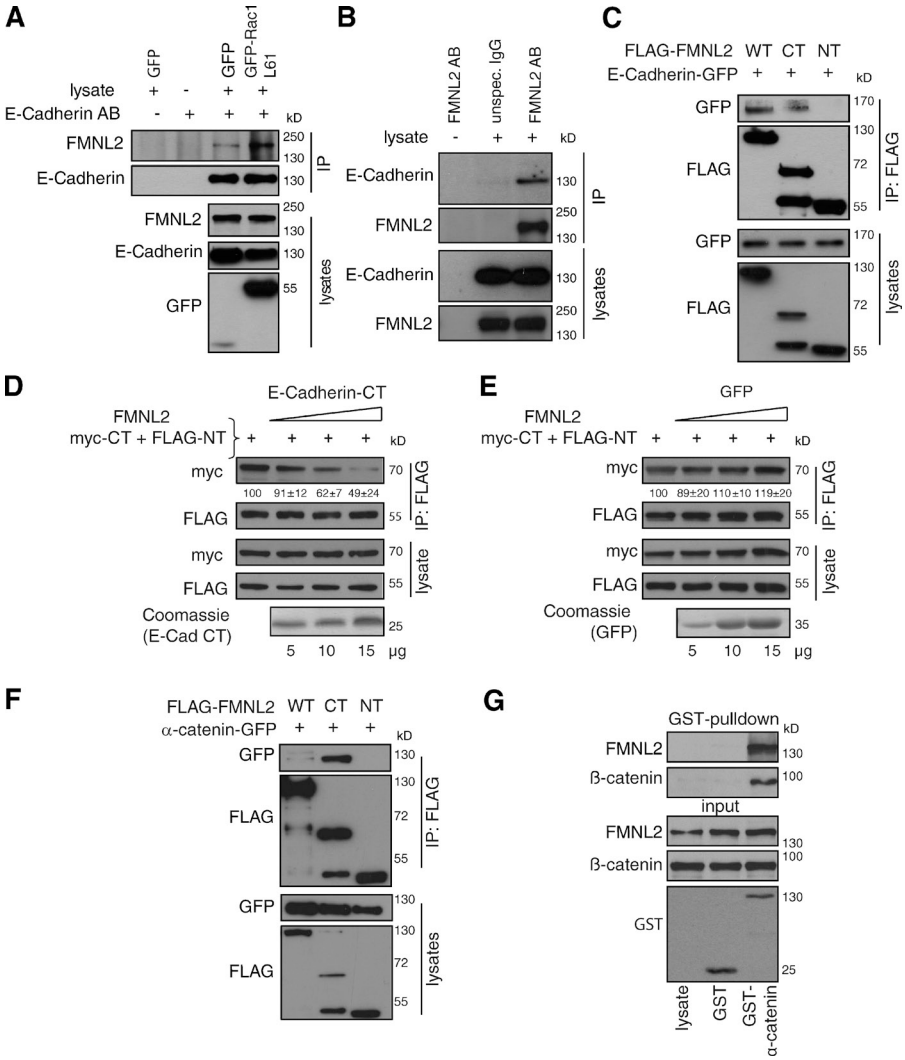

Figure 3. **FMNL2 associates with AJ components.** (A) E-Cadherin was immunoprecipitated (IP) from cells expressing GFP or GFP-Rac1-L61 to test for coprecipitation of FMNL2 by immunoblotting. (B) Detection of endogenous E-Cadherin in immunoprecipitations of FMNL2 from wild-type MCF10A cells by immunoblotting. (C) HEK cells were transfected with E-Cadherin–GFP and FLAG-tagged FMNL2 derivatives. FLAG-tagged proteins were precipitated and bound GFP-tagged protein was detected by immunoblotting. (D) HEK cells were transfected with FLAG-FMNL2 N terminus (NT) and myc-FMNL2 CT. FLAG-FMNL2 NT was precipitated and tested for coprecipitation of myc-FMNL2 CT in the presence of increasing amounts of E-Cadherin CT. Purified E-Cadherin CT peptide was visualized by Coomassie staining. Numbers indicate statistical values ($n = 3$, means ± SD) obtained by quantification of coprecipitated myc-FMNL2 CT. (E) Control experiment to C using purified GFP. (F) Experiments were performed as in Fig. 3 B with α-catenin–GFP. (G) GST or GST–α-catenin were purified from bacterial lysates and incubated with MCF10A cell lysate. GST–α-catenin pulled down endogenous FMNL2 as well as β-catenin.

wondered whether regulation of FMNL2 autoinhibition modulates coimmunoprecipitation with E-Cadherin. We used FLAG-NT and myc-CT to reconstitute the inactive conformation of FMNL2 (Kitzing et al., 2010). Notably, titration of E-Cadherin-CT peptide to FMNL2-NT/-CT resulted in its dissociation, indicating that the FMNL2 CT must be accessible for association with E-Cadherin (Fig. 3 D). As a control, GFP peptide additions had no effect (Fig. 3 E).

In keratinocytes, formin-1 has been shown to bind α-catenin (Kobielak et al., 2004). We thus asked if the association of FMNL2 with the AJ complex involves binding to α-catenin. Interestingly, FMNL2-CT, but not FMNL2-NT, associated with α-catenin–GFP in cell extracts (Fig. 3 F). Moreover, purified α-catenin–GST also associated with endogenous FMNL2 in GST pull-down experiments (Fig. 3 G). These data argue that FMNL2 associates with the AJ complex mediated by the FMNL2 CT.

Next, we generated an MCF10A cell line for inducible, constitutively active Rac1-L61 expression (Fig. 4 A). RhoC and Cdc42 were previously found to be able to interact with the FMNL2-GBD (Kitzing et al., 2010; Block et al., 2012), which suggests that the FMNL2 actin polymerizing ability may be targeted by different RhoGTPases depending on the cellular signaling context or task. Doxycycline-mediated expression of Rac1-L61 in 3D cell culture led to an increase of F-actin and localization of FMNL2-GFP at the cell–cell adhesion site (Fig. 4, B and C) as well as to the association between E-Cadherin and FMNL2 (Fig. 4 D), although at a seemingly lower rate as compared with the direct E-Cadherin binding partner β-catenin (Drees et al., 2005; Fig. 4 D). Thus, the association of FMNL2 and the AJ complex depends on Rac1 activity. However, the precise nature of how FMNL2 communicates with the multiprotein AJ complex and whether additional factors are involved requires future investigations.

Next, we tested whether Rac1 can principally interact with FMNL2. Many formins have been shown to display a significant degree of GTPase binding diversity depending on the cellular and physiological context (Baarlink et al., 2010; Kühn and Geyer, 2014). In particular, Rac1 was proposed to bind to more than six members of the formin family, including FMNL1, mDia1 and -2, or DAAM1 (Kühn and Geyer, 2014). For this, we performed GST-FMNL2-GBD pulldown experiments, which confirmed RhoC binding as a control but further revealed an interaction with Rac1-L61 as well (Kitzing et al., 2010; Block et al., 2012; Fig. 4 E). These data suggest that FMNL2, in addition to other Rho-GTPases, can be targeted by Rac1 in cells.

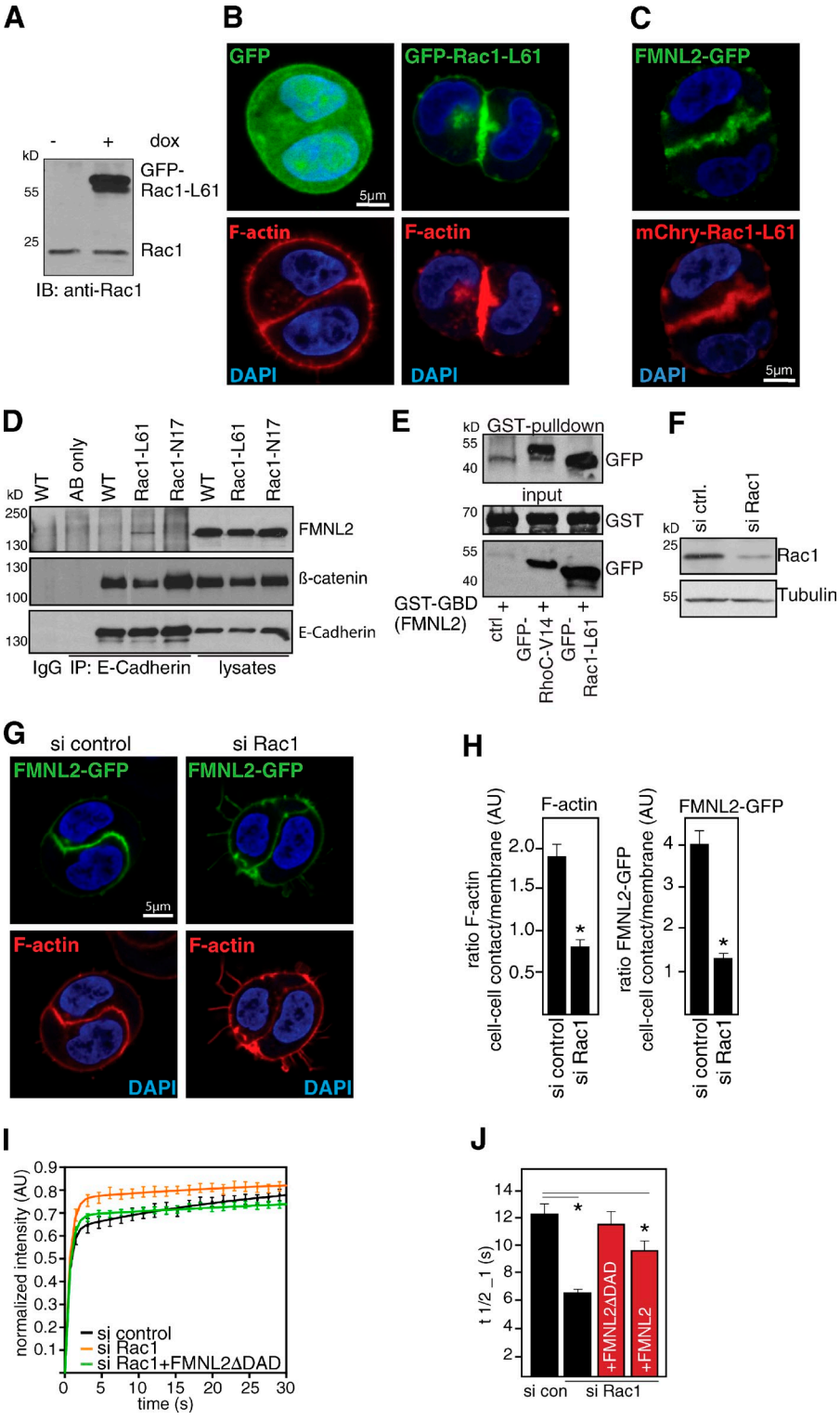

Figure 4. **Rac1 controls localization and function of FMNL2 at the cell–cell interface.** (A) Western blot of dox-inducible GFP-Rac1 expression in MCF10A. (B) MCF10A cells expressing GFP or GFP-Rac1-L61 were seeded in 3D and stained for F-actin. (C) Confocal image of MCF10A cells expressing mCherry-Rac1-L61 and FMNL2-GFP in 3D. (D) Immunoprecipitations (IP) of endogenous E-Cadherin were obtained from MCF10A cells induced to express GFP, GFP-Rac1-L61, or GFP-Rac1-N17. Precipitates were equally divided to test for FMNL2 or β-catenin by immunoblotting. An unspecific mouse IgG was used as a control. (E) GST pull-down assays showing an interaction between purified GST-FMNL2 GBD+FH3 and GFP-Rac1-L61 and GFP–RhoC-V14 expressed in HEK cells. (F) Western blot demonstrating Rac1 siRNA efficiency in MCF10A cells. (G) Confocal image of MCF10A FMNL2-GFP–expressing cells transfected with the indicated siRNAs and stained for F-actin. (H) Quantification of intensity ratios of F-actin or FMNL2-GFP based on line scans of confocal images as shown in G. (I) FRAP analysis in MCF10A GFP-actin cells treated with the indicated siRNAs. Expression of mCherry-FMNL2ΔDAD rescues the effect of Rac1 silencing. (J) Statistical analysis of I. Error bars indicate SEM. *, $P \leq 0.05$.

Activation of Rac1 steers FMNL2-mediated junctional actin assembly

We then determined the localization of FMNL2 after Rac1 siRNA. Rac1-depleted MCF10A cells seeded in 3D revealed a marked redistribution of FMNL2-GFP toward the peripheral plasma membrane, corresponding with a significant decrease in F-actin at the AJ (Fig. 4, F–H). Furthermore, Rac1 depletion altered the localization pattern of E-Cadherin–GFP (Fig. S1 K). Suppression of FMNL2 also partially interfered with E-Cadherin localization (Fig. S1 L). However, FRAP analysis of E-Cadherin–GFP after FMNL2 depletion was unaffected, which suggests that FMNL2 does not influence E-Cadherin turnover at AJs (Fig. S1 M).

The GFP-actin FRAP experiments show that suppression of Rac1 displays similar changes in actin turnover as compared with cells treated with FMNL2 siRNA (Fig. 4 I). To verify the

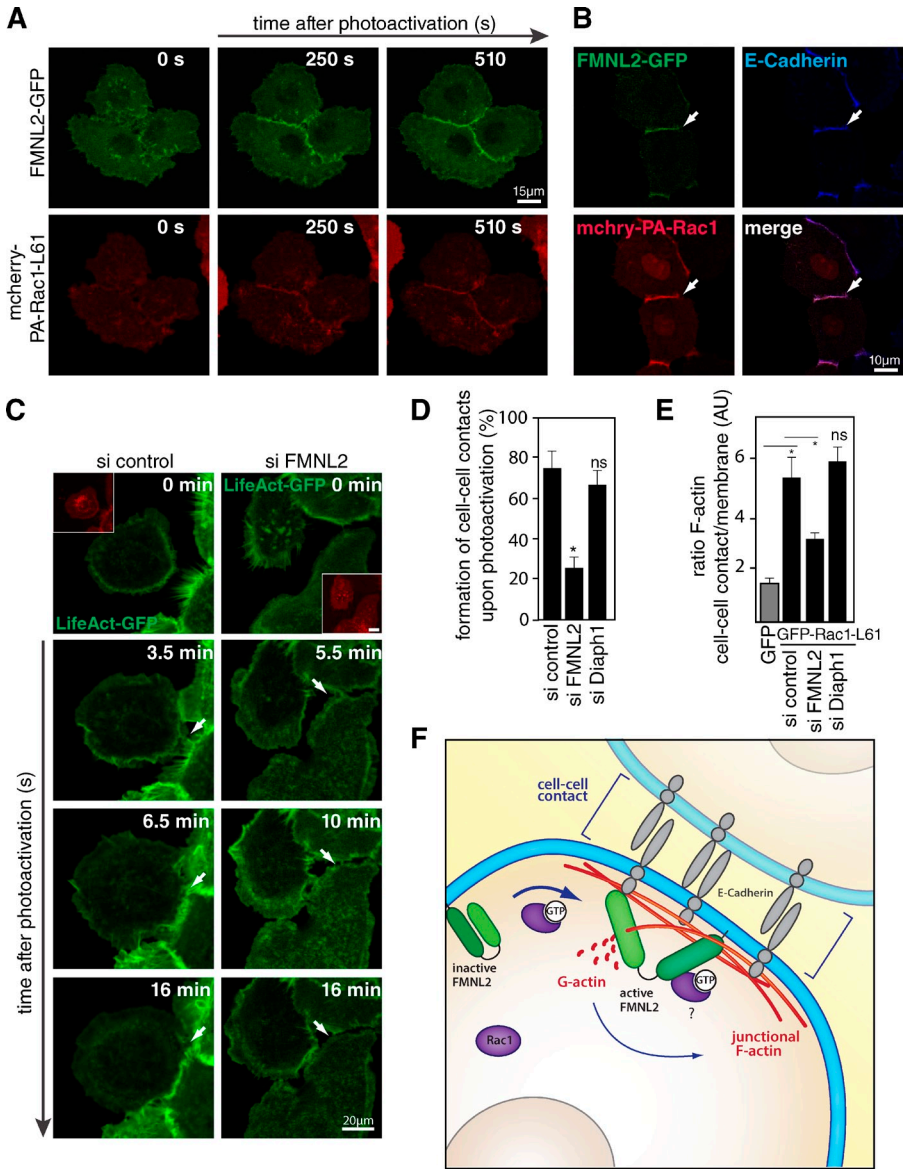

Figure 5. **FMNL2-driven actin assembly rapidly induces de novo cell–cell adhesion formation in response to Rac1 activation.** (A) Photoactivation of mCherry-PA-Rac1 in MCF10A cells coexpressing FMNL2-GFP. Rac-1 activity was uncaged through the irradiation, with 488-nm laser light simultaneously exciting FMNL2-GFP. (B) MCF10A cells expressing FMNL2-GFP and mCherry-PA-Rac1 were exposed to blue light for 16 min prior to labeling of E-Cadherin. (C) Time-lapse imaging of MCF10A cells expressing mCherry-PA-Rac1 and LifeAct-GFP transfected with the indicated siRNAs. Compared with control cells, FMNL2 suppression resulted in impaired contact formation (arrows). Insets show mCherry-PA-Rac1 expression (bar, 2 µm). (D) Quantification of C. (E) Quantification of junctional F-actin ratios obtained by line scan profiles from induced GFP- or GFP-Rac1-L61–expressing MCF10A transfected with the indicated siRNAs as in Fig. 4 B. (F) Cartoon illustrating the function of FMNL2. In the presence of active Rac1, FMNL2 becomes localized to the cell–cell contact area, where it associates with the adhesion complex to participate in junctional actin assembly. Error bars indicate SEM. *, $P \leq 0.05$.

involvement of FMNL2 in Rac1-mediated rearrangement of junctional actin, we investigated whether FMNL2ΔDAD can rescue Rac1 depletion. Indeed, FMNL2ΔDAD restored actin turnover in Rac1-depleted cells (Fig. 4, I and J), whereas full-length FMNL2 only partially did (Fig. 4 J). This implies that Rac1-mediated FMNL2 activation represents a critical step for junctional actin dynamics, which act upstream of FMNL2 association with and modulation by E-Cadherin.

Optogenetic regulation of Rac1 reveals rapid FMNL2-mediated AJ formation

The involvement of active RhoGTPases in cell–cell adhesion is controlled in a spatio-temporal manner (Yamada and Nelson, 2007). To elucidate the consequences of Rac1 activation on recruitment and regulation of FMNL2 at cell–cell contacts in real time, we made use of a photoactivatable LOV2-Rac1 (PA-Rac1) previously shown to promote lamellipodia formation (Wu et al., 2009). Strikingly, light-activated PA-Rac1-mCherry rapidly redistributed to AJs in MCF10A cells, which was accompanied by dynamic relocalization of FMNL2-GFP to newly formed cell–cell contacts within 2–3 min (Fig. 5, A and B; and Video 5). PA-Rac1–induced lamellipodia formation allowed us to reliably trigger de novo actin assembly at nascent cell–cell contacts by monitoring LifeAct-GFP (Fig. 5 C and Video 6). Interestingly, PA-Rac1 activation in FMNL2-silenced cells still resulted in lamellipodia formation with cells approaching each other; however, these cells were strongly impaired in establishing cell–cell contacts (Fig. 5, C and D; and Video 7), in contrast to Dia1-silenced cells (Fig. 5 D).

We then assessed whether 3D junctional F-actin assembly driven by Rac1 involves FMNL2. Indeed, accumulation of junctional F-actin in response to Rac1-L61 induction was significantly reduced in FMNL2 silenced cells as compared with cells depleted for Dia1 (Fig. 5 E). Together these data argue that FMNL2-mediated actin assembly drives nascent cell–cell contact formation downstream of Rac1 (Fig. 5 F).

Here, we identified the formin FMNL2 as a regulator of junctional actin assembly in human epithelial cells. Consistently,

FMNL2 is widely expressed and enriched in various human epithelial tissues (Gardberg et al., 2010). Rac1 activation triggers localization as well as the function of FMNL2 at AJs. In previous studies, Rac1 has been implicated in AJ formation via regulation of Arp2/3 (Kraemer et al., 2007; Verma et al., 2012). Interestingly, recent in vitro experiments showed that FMNL2 efficiently elongates filaments generated by the Arp2/3 complex (Block et al., 2012). It hence remains a future task to investigate whether FMNL2 and Arp2/3 synergistically control junctional F-actin assembly or if they regulate different pools or steps of actin turnover at AJs.

Materials and methods

Reagents, antibodies, and plasmids

Cell culture reagents were purchased from Invitrogen. Common reagents were from Sigma-Aldrich if not stated otherwise. Antibodies used were purchased from BD (mouse anti–E-Cadherin #610182, mouse anti–β-catenin #610153, mouse anti-Dia1 #610849, and mouse anti-Rac1 #610651), Sigma-Aldrich (rabbit anti-FMNL2 HPA005464, HRP-tagged anti-FLAG M2 and anti-myc antibodies), Cell Signaling Technology (rabbit anti-tubulin 11H10), Santa Cruz Biotechnology, Inc. (mouse anti-GFP B20, normal mouse and rabbit IgG), Bio-Rad Laboratories, Inc. (anti-rabbit-HRP), GE Healthcare (anti–mouse-HRP), Life Technologies (anti–mouse Alexa Fluor 488, anti–rabbit Alexa Fluor 647), or Jackson ImmunoResearch Laboratories, Inc. (rabbit-FITC).

All FMNL2 derivatives used were based on human FMNL2. Full-length FMNL2 (aa 1–1,092), FMNL2 CT (aa 521–1,092), or FMNL2 NT (aa 23–484) were transiently expressed under control of the EF-1 α promotor of the pEF-FLAG or pEF-myc vectors (previously described in Kitzing et al., 2010). For bacterial purification, FMNL2 GBD+FH3 (aa 23–484) was expressed under control of the tac promotor of the pGEX-KG vector. For stable expression of fluorescently tagged full-length FMNL2 or FMNL2ΔDAD (aa 1–1,045), the corresponding cDNAs were cloned into pEFGP-N1 or pmCherry-N1 (Takara Bio Inc.) and subcloned into pWXPL (EF-1 α promotor) using the MssI–SpeI restriction sites. EGFP-tagged human β-actin in the pcDNA3 backbone (B. Imhof, University of Geneva, Geneva, Switzerland) was subcloned into pWXPL. pWPXL-mCherry-PA-Rac1-L61 was obtained by subcloning the entire coding sequence of pTriEx-mCherry-PA-Rac1-L61 (T7 promotor; Wu et al., 2009) into the pWPXL backbone using MluI/SpeI.

The pEGFP-C2-α-catenin plasmid (CMV promotor, a gift from E. Sahai, Cancer Research UK, London, England, UK) was used for transient expression in mammalian cells and to generate pGEX6.1-α-catenin for bacterial purification (aa 1–906). The pCDNA3.1–E-Cadherin–GFP expression plasmid (human E-Cadherin under a CMV promotor; Addgene) was used to generate E-Cadherin variants. For bacterial purification, E-Cadherin cDNA comprising bp 2,134–2,694 was cloned into pGEX6.1 (tac promotor). To allow for doxycycline-inducible protein expression, cDNAs encoding GFP only, full-length E-Cadherin–GFP, mCherry/GFP-Rac1-L61, or GFP-Rac1-N17 (amplified from pCB6-GFP-Rac1 L61/N17; M. Way, Cancer Research UK) were inserted into the pInducer20 plasmid (TER2 promotor; Meerbrey et al., 2011) by homologous recombination using the Gateway technology (Invitrogen).

For the generation of inducible shRNA-expressing MCF10A cells, two sequences further referred to as shFMNL2 #1 (5′-TGCTGTTGACAGTGAGCGAGCTTCTATGCAGTTTATTAATTAGTGAAGCCACAGATGTAATTAATAAACTGCATAGAAGCCTGCCTACTGCCTCGGA-3′, V2LHS_161463) and shFMNL2 #2 (5′-TGCTGTTGACAGTGAGCGACTGATGAAATATGTAAAGCTATAGTGAAGCCACAGATGTATAGCTTTACATATTTCATCAGCTGCCTACTGCCTCGGA-3′, V2LHS_384851; GE Healthcare) were chosen after knockdown efficiency validation and were subsequently cloned into pInducer10 using the XhoI–MluI restriction sites. Furthermore, the nonsilencing pGIPZ control shRNA (5′-TGCTGTTGACAGTGAGCGATCTCGCTTGGGCGAGAGTAAGTAGTGAAGCCACAGATGTACTTACTCTCGCCCAAGCGAGAGTGCCTACTGCCTCGGA-3′), which was a gift from T. Stiewe (University of Marburg, Marburg, Germany), was transferred into the pInducer10. The pInducer plasmid was provided by G. Hu (National Institute of Environmental Health Sciences, Research Triangle Park, NC).

Cell culture, 3D cell culture, transfection, inhibitors, and viral transduction

Human HEK 293 or HEK 293T cells were maintained in DMEM supplemented with 10% fetal bovine serum, 2 mM glutamine, 100 U/ml penicillin, and 100 g/ml streptomycin at 37°C in a CO_2 atmosphere. Human MCF10A cells were cultured as described in Debnath et al. (2003). For 3D cell culture, 8-well μ-slides (Ibidi) were coated with growth factor reduced Matrigel (BD; diluted in serum-free medium to 2.5 mg/ml), and 20,000 cells were resuspended in 5 mg/ml Matrigel. For Caco-2 3D cell culture, μ-slides were coated with 100 µl of Matrigel. Approximately 50,000 Caco-2 cells were seeded in DMEM with 20% FCS and 2% Matrigel and maintained for 7 d. For long-term culturing of MCF10A cells, the 3-D Life Hydrogel system (Cellendes) was used. In short, chemically defined maleimide polymers were incubated with cross-linkers carrying thiol groups, which then polymerize into a gel-like network. Furthermore, RGD peptides were added that mimic components of the extracellular matrix. MCF10A cells (3,000 cells per 8 wells) were seeded and cultured for 14 d with medium changes every 2 d (MCF10A assay medium containing 5 ng/ml EGF and 333 ng/ml doxycycline).

For gene silencing, MCF10A cells were transfected with siRNA oligonucleotides (QIAGEN) using Lipofectamine RNAiMax (Invitrogen) according to the manufacturer's instructions. The following Flexitube siRNAs were used: HS_FMNL2_6 (5′-CAAATTAGGCCTGGACGAATA-3′), HS_FMNL2_8 (5′-TGGGACTAGATGGCCCACTAA-3′), HS_FMNL2_9 (5′-CTGCGGGCACATTCCCATAAA-3′), HS_DIAPH1_1 (5′-AAGATATGAGAGTGCAACT-3′), HS_DIAPH2_1 (5′-ACCGTCGAAAGCGGATTCC-3′), HS_DIAPH3_6 (5′-CCCATCGCCTTGAAGATATTA-3′), HS_FMNL1_6 (5′-CAAGCAGACGCTGCTGCACTA-3′), HS_FHOD1_2 (5′-CAGCGAGAGGAGCATCTACAA-3′), HS_RAC1_6 (5′-ATGCATTTCCTGGAGAATATA-3′), HS_CDH1_12 (5′-CTAGGTATTGTCTACTCTGAA-3′), and negative control siRNA (5′-AATTCTCCGAACGTGTCACGT-3′). For 3D siRNA and photoactivation experiments, the cells were transfected in cell culture dishes, seeded into Matrigel or glass bottom dishes the following day, and analyzed after 24 h.

HEK 293/T cells were transfected using the calcium phosphate method. For lentivirus production, HEK293T cells were cotransfected with the lentiviral packaging vectors psPAX/pMDG.2 and the pInducer or pWXPL plasmids. The lentiviral packing plasmids and pWPXL were provided by J. Swiercz (Max Planck Institute for Heart and Lung Research, Bad Nauheim, Germany). After 48 h, supernatants containing viral particles were harvested and filtered, and MCF10A cells were transduced using this supernatant containing 10 µg/ml hexadimethrine. MCF10A cells transduced with the pInducer10 shRNA system were then selected with 0.25 µg/ml puromycin followed by cell sorting. pInducer-transduced cells were induced using 333 ng/ml doxycycline. LifeAct-GFP and -mCherry lentiviral particles were a gift from O. Fackler (University of Heidelberg, Heidelberg, Germany).

Where indicated, cells were treated with the following inhibitors diluted in serum-free medium: 1 µM Latrunculin B was used and experiments were performed rapidly. Jasplakinolide (Santa Cruz Biotechnology, Inc.) was used at 0.5 µM, and cells were preincubated for 1 h. The Arp2/3 complex inhibitor I (CK-666) and the inactive control (CK-689; EMD Millipore) were used at 100 µM. Cells were preincubated for 1 h before analysis.

Live cell imaging, FRAP, and photoactivation

All microscopy was performed using an LSM 700 confocal laser scanning microscope equipped with a 63×/1.4 NA oil objective lens (Carl Zeiss). Live cell recordings of GFP- or mCherry-tagged proteins were performed in MCF10A medium at 37°C in a CO_2 humidified incubation chamber (Pecon, CO_2 module S1) using the time series setting of the ZEN software (Carl Zeiss).

For 3D reconstructions, MCF10A were seeded into Matrigel and monitored as z stacks every 3 min. 3D reconstructions were generated using the Zen software (Carl Zeiss). For live-cell imaging experiments in LifeAct-GFP and shRNA-expressing cells, five cells per condition were monitored for 10 min ($n = 3$).

FRAP experiments were performed at a 2× digital magnification. Stable GFP-actin–expressing MCF10A cells were seeded in Matrigel and analyzed after 24 h. For data normalization, a prebleached image was recorded. The junctional membrane was photobleached in a constant circular ROI (2 μm^2) by a 488-nm pulse at the highest laser power (100%). Recovery was followed by time-lapse acquisition at low laser power (70 frames at 1.5-s intervals for GFP-actin). Recovery was described by the function:

$$F(t) = \frac{F_{tot}^{PB}}{F_{jm}^{PB}} \times \frac{F_{jm}(t)}{F_{tot}(t)},$$

where F^{PB} indicates the fluorescence measured before bleaching of the junctional membrane (*jm*) or on the entire cell (*tot*) to correct for bleaching caused by imaging (Brandt et al., 2009). Table S1 summarizes the number of recordings and data analysis. If the junctional actin pool was discontinuous, remaining GFP-actin at the cell–cell contact was bleached. For illustration purposes, FRAP time curves are cropped at 30 s; see Fig. 2 G for an example of a 90-s recording. FRAP data were analyzed using the ZEN software (Carl Zeiss).

Optogenetic protein activation was essentially performed as described previously (Baarlink et al., 2013). In brief, cells were seeded at subconfluency on 35-mm glass-bottom dishes (In Vitro Scientific). Throughout experiments, mCherry-LA-Rac1 was activated using the 488 nm laser at >1% laser power, which allowed simultaneously recording of the GFP signal. The effects of PA-Rac1 activation were recorded for up to 200 frames at 5-s intervals. For quantification, cells with a distance of up to 15 µm prior to illumination were considered. Cell–cell contact formation was assessed through LifeAct-GFP after 16 min of irritation (n = 3, >15 cells per condition).

Immunostainings, scratch wound assay, proliferation assay, quantification, and image analysis

The immunostaining protocol of MCF10A cells in Matrigel was adapted from Debnath et al. (2003). In brief, MCF10A cells in the gel were fixed with 8% formaldehyde/PBS and permeabilized using 0.3% Triton X-100/PBS. For visualization of the actin cytoskeleton, the cells were incubated with Phalloidin–Alexa Fluor 488 or Phalloidin-rhodamine (1:800 in PBS; Invitrogen). For antibody labeling, the cells were blocked (5% goat serum, 0.4% glycerol, 0.1% BSA, 0.04% sodium azide, and 0.2% Triton X-100) and then incubated with the primary antibodies overnight. DAPI for staining nuclei was used 1:10,000 in PBS.

Wound scratch assays were performed as described in Goulimari et al. (2005). In brief, induced shRNA-expressing MCF10A cells were seeded to confluency on coverglass. The monolayer was wounded and the cells were fixed and stained for tubulin or phalloidin. Localization of the microtubule organization center (MTOC) was quantified as in Goulimari et al. (2005).

WST proliferation assays were performed according to the manufacturer's instructions (WST-1; Roche).

The ratio of F-actin intensity between the plasma membrane and the membrane of the junctional area was quantified using the line scan function in the ZEN software (Carl Zeiss). For this, the maximal intensity of the three top peaks was determined and the ratio between the mean of the outer membranes and the junctional area was calculated (see Fig. 1, H and I). For each condition, at least 30 cells were quantified, as derived from three experiments.

Coimmunoprecipitations and protein purification

Cells were lysed in RIPA buffer (50 mM Tris, 150 mM NaCl, 2 mM EDTA, 0.1% Triton X-100, 0.25% DOC, and 0.1% SDS) supplemented with protease inhibitors (Roche) for all coimmunoprecipitation experiments. Transfections in HEK cells were performed in 10-cm dishes, which were lysed and incubated with precoupled agarose beads for 1 h at 4°C. For endogenous coimmunoprecipitations, MCF10A cells of 1–2 T75 flasks were scraped and incubated with protein A/G agarose beads (Santa Cruz Biotechnology, Inc.), which were preincubated with 1 µg of antibody for 1 h at 4°C. All types of beads were then washed, and the eluted proteins were subjected to Western blotting. Protein purifications and GST pull-down were performed as described in Kitzing et al. (2010). In brief, transformed BL21/De *E. coli* were collected and lysed (50 mM Tris, pH 8, 100 mM NaCl, and protease inhibitor). Proteins were purified using glutathione beads and eluted (50 mM Tris, pH 8, 100 mM NaCl, and 20 mM glutathione). PreScission Protease (Sigma-Aldrich) was used for protein cleavage. For GST pull-down experiments, purified proteins were coupled to glutathione beads and whole cell lysates of MCF10A or transfected HEK cells were incubated with the beads for 1 h at 4°C. Protein complexes were eluted using Laemmli buffer and subjected to Western blotting.

Real-time reverse-transcription PCR

For total RNA extraction, TRIzol reagent was used according to the manufacturer's instructions. The reverse transcription was performed using Revert Aid Reverse transcription (Fermentas) and quantified using the SYBR green system (Bio-Rad Laboratories). Primers used for determination of formin expression in MCF10A are listed in Kitzing et al. (2010).

Statistical analysis

All statistical analyses were done using GraphPad Prism 4 (GraphPad Software Inc.). Data are expressed as mean ± SEM or SD. Error bars are shown as SEM. Statistical significance was evaluated with the unpaired Student t test. Statistical differences were judged significant at $P \leq 0.05$. Western blot quantification was performed using ImageJ (National Institutes of Health).

Online supplemental material

Fig. S1 includes additional data substantiating the role of FMNL2 and Rac1 in junctional actin regulation. Table S1 summarizes the statistical analysis of all FRAP data. Videos 1 and 2 show the dynamics of LifeAct-mCherry and E-Cadherin–GFP or FMNL2-GFP in dividing MCF10A cells forming a nascent cell–cell contact in Matrigel. Videos 3 and 4 compare junctional actin dynamics in MCF10A cell pairs seeded in Matrigel expressing control shRNA or shRNA against FMNL2, respectively. Video 5 shows that photoactivation of Rac1 leads to rapid localization of FMNL2 to the forming cell–cell contacts in MCF10A cells. Videos 6 and 7 depict the differences in cell–cell contact formation after Rac1 light activation in control and FMNL2 siRNA-treated cells. Online supplemental material is available at http://www.jcb.org/cgi/content/full/jcb.201412015/DC1.

We are grateful to H. Raifer from the Flow Cytometry Core Facility (Marburg) and G. Hu (National Institute of Environmental Health Sciences) for providing the pInducer system. We thank laboratory members for discussions and M. Losekam, F. Aktuna, A. Wüstenhagen, and N. Luther for technical assistance.

This work was funded by grants of the Deutsche Forschungsgemeinschaft to R. Grosse (GR 2111/8-1, SPP 1782).

The authors declare no competing financial interest.

Submitted: 3 December 2014
Accepted: 1 April 2015

References

Baarlink, C., D. Brandt, and R. Grosse. 2010. SnapShot: Formins. *Cell*. 142:172: e1. http://dx.doi.org/10.1016/j.cell.2010.06.030

Baarlink, C., H. Wang, and R. Grosse. 2013. Nuclear actin network assembly by formins regulates the SRF coactivator MAL. *Science*. 340:864–867. http://dx.doi.org/10.1126/science.1235038

Baker, B.M., and C.S. Chen. 2012. Deconstructing the third dimension: how 3D culture microenvironments alter cellular cues. *J. Cell Sci.* 125:3015–3024. http://dx.doi.org/10.1242/jcs.079509

Block, J., D. Breitsprecher, S. Kühn, M. Winterhoff, F. Kage, R. Geffers, P. Duwe, J.L. Rohn, B. Baum, C. Brakebusch, et al. 2012. FMNL2 drives actin-based protrusion and migration downstream of Cdc42. *Curr. Biol.* 22:1005–1012. http://dx.doi.org/10.1016/j.cub.2012.03.064

Brandt, D.T., C. Baarlink, T.M. Kitzing, E. Kremmer, J. Ivaska, P. Nollau, and R. Grosse. 2009. SCAI acts as a suppressor of cancer cell invasion through the transcriptional control of beta1-integrin. *Nat. Cell Biol.* 11:557–568. http://dx.doi.org/10.1038/ncb1862

Breitsprecher, D., and B.L. Goode. 2013. Formins at a glance. *J. Cell Sci.* 126:1–7. http://dx.doi.org/10.1242/jcs.107250

Campellone, K.G., and M.D. Welch. 2010. A nucleator arms race: cellular control of actin assembly. *Nat. Rev. Mol. Cell Biol.* 11:237–251. http://dx.doi.org/10.1038/nrm2867

Carramusa, L., C. Ballestrem, Y. Zilberman, and A.D. Bershadsky. 2007. Mammalian diaphanous-related formin Dia1 controls the organization of E-cadherin-mediated cell-cell junctions. *J. Cell Sci.* 120:3870–3882. http://dx.doi.org/10.1242/jcs.014365

Cavey, M., and T. Lecuit. 2009. Molecular bases of cell-cell junctions stability and dynamics. *Cold Spring Harb. Perspect. Biol.* 1:a002998. http://dx.doi.org/10.1101/cshperspect.a002998

Debnath, J., and J.S. Brugge. 2005. Modelling glandular epithelial cancers in three-dimensional cultures. *Nat. Rev. Cancer*. 5:675–688. http://dx.doi.org/10.1038/nrc1695

Debnath, J., S.K. Muthuswamy, and J.S. Brugge. 2003. Morphogenesis and oncogenesis of MCF-10A mammary epithelial acini grown in three-dimensional basement membrane cultures. *Methods*. 30:256–268. http://dx.doi.org/10.1016/S1046-2023(03)00032-X

Drees, F., S. Pokutta, S. Yamada, W.J. Nelson, and W.I. Weis. 2005. α-Catenin is a molecular switch that binds E-cadherin-β-catenin and regulates

actin-filament assembly. *Cell*. 123:903–915. http://dx.doi.org/10.1016/j.cell.2005.09.021

Gardberg, M., K. Talvinen, K. Kaipio, K. Iljin, C. Kampf, M. Uhlen, and O. Carpén. 2010. Characterization of Diaphanous-related formin FMNL2 in human tissues. *BMC Cell Biol.* 11:55. http://dx.doi.org/10.1186/1471-2121-11-55

Goulimari, P., T.M. Kitzing, H. Knieling, D.T. Brandt, S. Offermanns, and R. Grosse. 2005. Gα12/13 is essential for directed cell migration and localized Rho-Dia1 function. *J. Biol. Chem.* 280:42242–42251. http://dx.doi.org/10.1074/jbc.M508690200

Ivanov, A.I., D. Hunt, M. Utech, A. Nusrat, and C.A. Parkos. 2005. Differential roles for actin polymerization and a myosin II motor in assembly of the epithelial apical junctional complex. *Mol. Biol. Cell*. 16:2636–2650. http://dx.doi.org/10.1091/mbc.E05-01-0043

Jou, T.S., and W.J. Nelson. 1998. Effects of regulated expression of mutant RhoA and Rac1 small GTPases on the development of epithelial (MDCK) cell polarity. *J. Cell Biol.* 142:85–100. http://dx.doi.org/10.1083/jcb.142.1.85

Kitzing, T.M., Y. Wang, O. Pertz, J.W. Copeland, and R. Grosse. 2010. Formin-like 2 drives amoeboid invasive cell motility downstream of RhoC. *Oncogene*. 29:2441–2448. http://dx.doi.org/10.1038/onc.2009.515

Kobielak, A., H.A. Pasolli, and E. Fuchs. 2004. Mammalian formin-1 participates in adherens junctions and polymerization of linear actin cables. *Nat. Cell Biol.* 6:21–30. http://dx.doi.org/10.1038/ncb1075

Kovacs, E.M., S. Verma, R.G. Ali, A. Ratheesh, N.A. Hamilton, A. Akhmanova, and A.S. Yap. 2011. N-WASP regulates the epithelial junctional actin cytoskeleton through a non-canonical post-nucleation pathway. *Nat. Cell Biol.* 13:934–943. http://dx.doi.org/10.1038/ncb2290

Kraemer, A., M. Goodwin, S. Verma, A.S. Yap, and R.G. Ali. 2007. Rac is a dominant regulator of cadherin-directed actin assembly that is activated by adhesive ligation independently of Tiam1. *Am. J. Physiol. Cell Physiol.* 292:C1061–C1069. http://dx.doi.org/10.1152/ajpcell.00073.2006

Kühn, S., and M. Geyer. 2014. Formins as effector proteins of Rho GTPases. *Small GTPases*. 5:e29513. http://dx.doi.org/10.4161/sgtp.29513

Kutys, M.L., A.D. Doyle, and K.M. Yamada. 2013. Regulation of cell adhesion and migration by cell-derived matrices. *Exp. Cell Res.* 319:2434–2439. http://dx.doi.org/10.1016/j.yexcr.2013.05.030

Meerbrey, K.L., G. Hu, J.D. Kessler, K. Roarty, M.Z. Li, J.E. Fang, J.I. Herschkowitz, A.E. Burrows, A. Ciccia, T. Sun, et al. 2011. The pINDUCER lentiviral toolkit for inducible RNA interference in vitro and in vivo. *Proc. Natl. Acad. Sci. USA*. 108:3665–3670. http://dx.doi.org/10.1073/pnas.1019736108

Michael, M., and A.S. Yap. 2013. The regulation and functional impact of actin assembly at cadherin cell-cell adhesions. *Semin. Cell Dev. Biol.* 24:298–307. http://dx.doi.org/10.1016/j.semcdb.2012.12.004

Nakagawa, M., M. Fukata, M. Yamaga, N. Itoh, and K. Kaibuchi. 2001. Recruitment and activation of Rac1 by the formation of E-cadherin-mediated cell-cell adhesion sites. *J. Cell Sci.* 114:1829–1838.

Niessen, C.M., D. Leckband, and A.S. Yap. 2011. Tissue organization by cadherin adhesion molecules: dynamic molecular and cellular mechanisms of morphogenetic regulation. *Physiol. Rev.* 91:691–731. http://dx.doi.org/10.1152/physrev.00004.2010

Ratheesh, A., and A.S. Yap. 2012. A bigger picture: classical cadherins and the dynamic actin cytoskeleton. *Nat. Rev. Mol. Cell Biol.* 13:673–679. http://dx.doi.org/10.1038/nrm3431

Tang, V.W., and W.M. Brieher. 2012. α-Actinin-4/FSGS1 is required for Arp2/3-dependent actin assembly at the adherens junction. *J. Cell Biol.* 196:115–130. http://dx.doi.org/10.1083/jcb.201103116

Tardy, Y., J.L. McGrath, J.H. Hartwig, and C.F. Dewey. 1995. Interpreting photoactivated fluorescence microscopy measurements of steady-state actin dynamics. *Biophys. J.* 69:1674–1682. http://dx.doi.org/10.1016/S0006-3495(95)80085-8

Vaillant, D.C., S.J. Copeland, C. Davis, S.F. Thurston, N. Abdennur, and J.W. Copeland. 2008. Interaction of the N- and C-terminal autoregulatory domains of FRL2 does not inhibit FRL2 activity. *J. Biol. Chem.* 283:33750–33762. http://dx.doi.org/10.1074/jbc.M803156200

Verma, S., S.P. Han, M. Michael, G.A. Gomez, Z. Yang, R.D. Teasdale, A. Ratheesh, E.M. Kovacs, R.G. Ali, and A.S. Yap. 2012. A WAVE2-Arp2/3 actin nucleator apparatus supports junctional tension at the epithelial zonula adherens. *Mol. Biol. Cell*. 23:4601–4610. http://dx.doi.org/10.1091/mbc.E12-08-0574

Weis, W.I., and W.J. Nelson. 2006. Re-solving the cadherin-catenin-actin conundrum. *J. Biol. Chem.* 281:35593–35597. http://dx.doi.org/10.1074/jbc.R600027200

Wu, Y.I., D. Frey, O.I. Lungu, A. Jaehrig, I. Schlichting, B. Kuhlman, and K.M. Hahn. 2009. A genetically encoded photoactivatable Rac controls the motility of living cells. *Nature*. 461:104–108. http://dx.doi.org/10.1038/nature08241

Yamada, S., and W.J. Nelson. 2007. Localized zones of Rho and Rac activities drive initiation and expansion of epithelial cell-cell adhesion. *J. Cell Biol.* 178:517–527. http://dx.doi.org/10.1083/jcb.200701058

Zhang, J., M. Betson, J. Erasmus, K. Zeikos, M. Bailly, L.P. Cramer, and V.M. Braga. 2005. Actin at cell-cell junctions is composed of two dynamic and functional populations. *J. Cell Sci.* 118:5549–5562. http://dx.doi.org/10.1242/jcs.02639